Journal of The Electrochemical Society, **159** (12) A1954-A1960 (2012)
0013-4651/2012/159(12)/A1954/7/$28.00 © The Electrochemical Society

In Situ Carbon Coated Li_2MnSiO_4/C Composites as Cathodes for Enhanced Performance Li-Ion Batteries

Akkisetty Bhaskar,[a] Melepurath Deepa,[a,z] T. N. Rao,[b] and U. V. Varadaraju[c]

[a]*Indian Institute of Technology Hyderabad, Yeddumailaram-502205, Andhra Pradesh, India*
[b]*Nanomaterials Center, ARCI, Hyderabad-500005, India*
[c]*Department of Chemistry, Indian Institute of Technology Madras, Chennai-600036, India*

An in-situ carbon coated Li_2MnSiO_4/C composite was synthesized by a nanocomposite gel precursor route using starch as the carbon source. Our approach enabled a uniform coating of amorphous carbon on Li_2MnSiO_4 with an orthorhombic crystalline structure, which was confirmed by electron microscopy, X-ray diffraction and Raman studies. Conducting-atomic force microscopy (C-AFM) images also revealed the presence of high current interconnected domains in the composite, indicating the ability of the carbon coating to facilitate electron movement. Galvanostatic charge-discharge studies demonstrated outstanding initial charge and discharge capacities, respectively, of 330 and 195 mAh g^{-1} at 0.05 C-rate for the composite, and after 30 cycles a reversible capacity of 115 mAh g^{-1} was retained. The electrochemical performance of the neat silicate was dismal (10.6 mAh g^{-1} at 0.05 C-rate), which again reiterated the role of carbon in improving the conduction and Li-ion storage capacity of the silicate. An insignificant change in charge transfer resistance, with cycling, as inferred from impedance spectroscopy illustrated that charge transfer and transport processes remain facile with cycling, thus demonstrating Li_2MnSiO_4/C to be promising cathode Li-ion batteries.
 [DOI: 10.1149/2.042212jes]

Manuscript submitted July 9, 2012; revised manuscript received September 6, 2012. Published October 1, 2012.

Lithium ion batteries are popular choices as power sources for a gamut of applications that include cell phones, laptop computers, digital cameras, hybrid electric vehicles and even for electric vehicles. Commercially available Li-ion batteries typically employ lithium transition metal oxides as the cathode material. However, upon charging to very high voltages, these oxides tend to behave as strong oxidizers (for instance, Co^{3+}/Co^{4+} and Mn^{3+}/Mn^{4+}) and release oxygen from the crystal lattice to the electrolyte solution which manifests in thermal runaway reactions.[1,2] As a consequence, these materials are unsafe for large-scale applications such as electric vehicles. Apart from safety concerns, the lithium cobalt oxide is expensive, toxic and less abundant. To circumvent these issues, poly(anion) based compounds like $LiFePO_4$ have been used as cathodes in Li-ion batteries, as they are safe and easy to handle.[3] However, these suffer from a major shortcoming, as their theoretical specific capacity is limited to 170 mAh g^{-1}, which corresponds to one electron (1 Li^+) reaction per formula unit. Contrasting this, lithium orthosilicates such as Li_2MSiO_4 (M = Mn, Fe, Co) are very safe and their theoretical specific capacity is also reasonably high i.e. above 300 mAh g^{-1} which corresponds to a two electron (2 Li^+) reaction. Of particular significance is Li_2MnSiO_4 as the Mn^{2+}/Mn^{4+} redox couple is ideal owing to its higher potential *versus* Li metal and therefore high energy density can be realized. Other advantage is the low cost of manganese. But Li_2MnSiO_4 inherently suffers from poor electronic conducting properties and incorporating carbon with the active battery material is a widely used method to improve conductivity. In comparison, in Li_2CoSiO_4, the limitation is that not only does the oxidation of the Co^{3+}/Co^{4+} occur at a high voltage (above 5 V) but the electrolyte is also susceptible to decomposition at such a high potential.[4,5] The toxicity of cobalt is also a drawback. In Li_2FeSiO_4, iron does not easily oxidize and reduce reversibly between +2 and +4 oxidation states (Fe^{2+}/Fe^{3+} and Fe^{3+}/Fe^{4+}) during the electrochemical reaction.[6–9]

There are several reports on Li_2MnSiO_4 synthesized by solid-state, sol-gel and hydrothermal methods wherein the effects of morphology and atomic arrangement of the orthosilicate on electrochemical properties of Li_2MnSiO_4 has been studied.[10–16] A Li_2MnSiO_4/C nanocomposite prepared by Li et al. involving a solution route showed a reversible capacity of 209 mAh g^{-1} corresponding to a 1.27 Li^+ insertion per one formula unit (FU), in the first cycle at a very low current density of 5 mA g^{-1}.[12] However, the composite suffered from poor cyclability as after 10 cycles the specific capacity reduced to 140 mAh g^{-1}. Similarly, a nanostructured Li_2MnSiO_4/C composite synthesized by a microwave-solvothermal route by Manthiram and co-workers showed a reversible specific capacity of 210 mAh g^{-1} (1.27 Li^+ per FU) in the first cycle at a 0.05 C-rate.[17] Authors observed a severe capacity fading as after 40 cycles a capacity of only 60 mAh g^{-1} was retained by the composite.[17] Recently, Aravindan et al. employed a conventional solid-state synthetic method, by using adipic acid as the carbon source and fabricated electrodes with altered carbon content.[18] Their cell delivered an initial reversible capacity of 160 mAh g^{-1} (~ 0.97 Li^+ per FU) and it exhibited a stable cycling response as even after 40 cycles the cell continued to deliver a capacity of 140 mAh g^{-1}. In another report, Rangappa et al. synthesized ultra-thin sheets of Li_2MnSiO_4 by supercritical solvothermal method followed by mechanical milling with poly(3,4-ethylenedioxythiophene) or PEDOT and multiwalled carbon nanotubes (MWNTs).[19] The cell showed an initial reversible capacity of 220 and 340 mAh g^{-1}, respectively, at 19 and 45°C in the voltage range of 1.5 to 4.8 V.[19] However authors obtained these values at a very low C-rate of 0.02. At room temperature, the capacity of their composite rapidly faded from 220 to 130 mAh g^{-1} after 10 cycles at 0.02 C-rate.[19] In a previous report by Basu et al., the first step involved the preparation of pristine Li_2MnSiO_4 by combustion method which was followed by the formation of Li_2MnSiO_4/C composite using ballmilling and solid-state sintering.[20] They observed an initial discharge capacity of 161 mAh g^{-1} (~ 0.97 Li^+ per FU) at very low current density of 10 mA g^{-1}. However, to the best of our knowledge, the use of starch as the carbon source for the formation of an in-situ carbon coated Li_2MnSiO_4/C composite has not been reported to date. It is also evident from the results on Li_2MnSiO_4 in literature, that generally low C-rates / high temperature have been employed to achieve higher capacities.[12,17,19]

Here, we report a facile nanocomposite gel precursor route for the synthesis of Li_2MnSiO_4/C composite by using starch as the carbon source. The advantages of this technique are that it is time saving, cost-effective and also allows for mass-scale production, which is a primary concern for commercial applications of Li-ion batteries. Furthermore, since a direct contact is established between the carbon source and the Li_2MnSiO_4 precursors, right at the onset of the synthetic process, the resulting sintered material is characterized by a uniform coating of carbon deposited over the Li_2MnSiO_4 grains. Our modified methodology, ensued in a homogeneous Li_2MnSiO_4/C composite which showed a remarkably high initial charge capacity of 330 mAh g^{-1} (which is close to the theoretical specific capacity of 333 mAh g^{-1} of Li_2MnSiO_4) at a 0.05 C-rate. In this report, we optimized the composite on the basis of starch concentration and annealing temperature and evaluated the optimized Li_2MnSiO_4/C composite in terms of crystal structure, morphology and

[z]E-mail: mdeepa@iith.ac.in

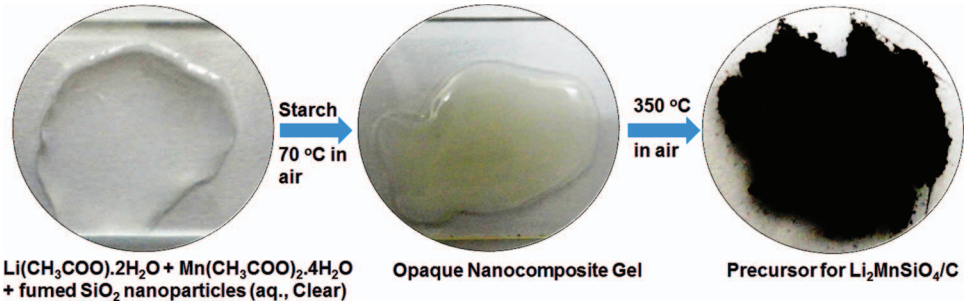

Scheme 1. Photographs of intermediates prior to formation of Li_2MnSiO_4/C nanocomposite.

conduction properties and correlated the same to its good electrochemical performance.

Experimental

Preparation of Li_2MnSiO_4/C composite.— The starting materials used for nanocomposite gel preparation of Li_2MnSiO_4 precursor were highly pure $Li(OCOCH_3).4H_2O$ (Alfa Aesar, 99.9%), $Mn(OCOCH_3)_2.4H_2O$ (Sigma, 99%), CAB-O-SIL fumed SiO_2 (dimensions: 10 nm) as a Si source and starch (Merck, 99%). To a solution of stoichiometric amounts (Li:Mn:Si:Starch = 2:1:1:1.33 molar ratio) of precursors, 20 mL of ultrapure water (obtained from Milli-Q) was added and stirred for 1 h at 70°C. A white gelatinous solution was obtained and it was fired at 350°C in a preheated electric oven for 5–10 min. Scheme 1 shows the photographs of the opaque nanocomposite gel and the black colored solid precursor generated by heating the gel at 350°C in air. The precusror was subsequently converted to the Li_2MnSiO_4/C composite. The resulting black powder was grinded for 1 h and post-annealed at 900°C, in an Ar atmosphere and a black solid of Li_2MnSiO_4/C composite was obtained. Neat Li_2MnSiO_4 was also prepared from a precursor sol containing the respective salts in a Li:Mn:Si = 2:1:1 molar ratio which was subjected to a pre-heat-treatment at 350°C followed by post-annealing at 900°C.

Characterization and Electrochemical Measurements.— X-ray diffraction (XRD) was performed on the samples using a PANalytical, X'Pert PRO, Netherlands with CuKα (λ = 1.5406 Å) radiation by applying an accelerating voltage of 40 V and 30 mA current. Morphological features of the samples were investigated using a field emission scanning electron microscope (FE-SEM Hitachi S-4300 SE/N). High resolution transmission electron microscopy (HRTEM) was performed on a JEOL 3010, 200 KV. Thermogravimetric analysis (TGA, TA instruments, Q600) was carried out on the Li_2MnSiO_4/C composites for quantifying the amount of carbon incorporated in the composites. BET isotherm (Quantachrom 2200) was used for surface area measurements. The working electrodes were prepared by mixing 80% of active material (Li_2MnSiO_4/C or neat Li_2MnSiO_4), 10% acetylene black and 10% Poly(vinylidene) fluoride (PVdF) with a few drops of N-methyl pyrrolidine. The resulting slurry was coated on 13 mm stainless steel foils and dried at 80°C for 12 h in a vacuum oven for expunging the solvent. Typically, the active material (Li_2MnSiO_4/C or Li_2MnSiO_4) weights were maintained in the range of 1.2 ± 0.4 mg cm^{-2}, on the electrodes for all electrochemical measurements. Swagelok cells were used for evaluating the Li-ion storage performance of the electrodes. The cells were assembled inside an argon filled glove-box wherein oxygen level of ≤ 1 ppm and moisture concentration of ≤ 0.5 ppm were maintained. A lithium foil was used as a counter electrode and a whatman glass microfiber filter paper was used as a separator. Commercially available $LiPF_6$ dissolved in a 1:1 molar ratio of ethylene carbonate and propylene carbonate (Merck) was employed as the electrolyte. Cyclic voltammetry and was performed on the two electrode Swagelok cells on an Autolab PGSTAT 302N coupled with NOVA 1.7 software at a scan rate of 0.05 mV s^{-1} at room temperature.

Electrochemical impedance spectra were also recorded for the cells using the same instrument, over a frequency range of 10 mHz to 100 KHz and under an ac amplitude of 10 mV. Galvanostatic charge-discharge measurements were performed on a battery testing unit (Arbin Instruments, BT 2000) at different current rates in appropriate voltage ranges *versus* Li/Li^+ at room temperature. Conductive AFM (C-AFM, Veeco, Multimode 8 with ScanAsyst) was used for collecting simultaneous topography and current images in contact mode. Cantilevers with a Pt/Ir tip and having a spring constant of 0.2 N/m were used. The current sensitivity was 1 nA V^{-1} and a load force of 50 nN was maintained between the tip and the sample. A coat of silver paste was used for taking contacts. The contact tip was scanned in contact with the sample surface. The z-feedback loop used the dc cantilever defending a signal to maintain a constant force between the tip and the sample to generate topography images. Simultaneously a dc bias of 50 mV was applied to the tip. The sample was held at ground potential. The built-in pre-amplified scanner head measured the current passing through the tip and sample and imaged the current profiles.

Results and Discussion

Structural Characterization.— Fig. 1 shows the TGA plot of Li_2MnSiO_4/C composites prepared from a sol containing 1 mol of starch. The TGA plot was recorded in air flow for the solid obtained after subjecting it to a final annealing treatment at 900°C for 10 h. The figure shows the weight loss in the Li_2MnSiO_4/C composite as a function of temperature in the range of 30–900°C. A total weight loss of ∼ 15% was registered and this loss corresponds to the weight percent of carbon coated on the Li_2MnSiO_4 particles.

Fig. 2a shows the XRD patterns of the neat Li_2MnSiO_4 and the Li_2MnSiO_4/C composite. To date, most of the reports on Li_2MnSiO_4

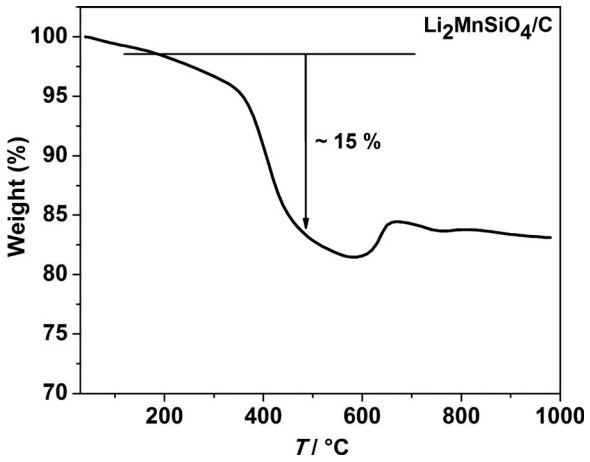

Figure 1. Thermogravimetric plot of the Li_2MnSiO_4/C composite synthesized from a sol containing 1 mol of starch.

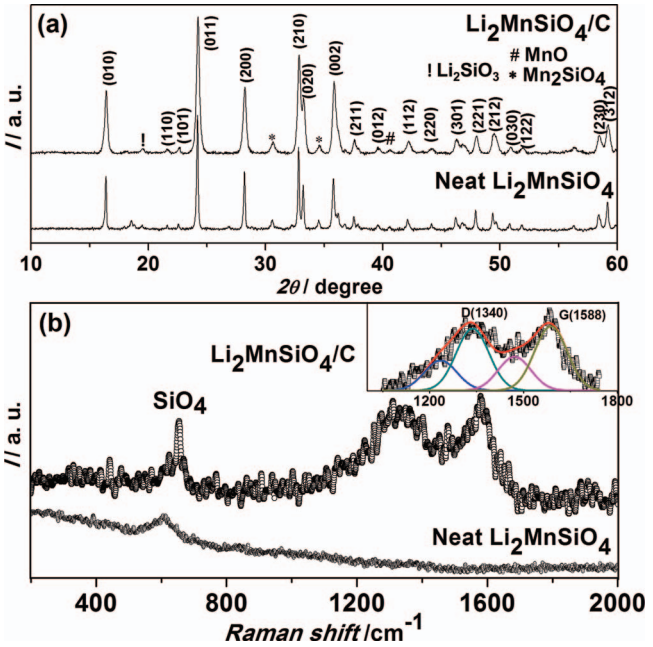

Figure 2. (a) XRD patterns of Li_2MnSiO_4/C composite and neat Li_2MnSiO_4 (b) Raman spectra of the Li_2MnSiO_4/C composite and neat Li_2MnSiO_4 in the 200–2000 cm^{-1} wavenumber region; inset of (b) shows the deconvoluted Raman spectrum in the range of 1000–1800 cm^{-1}.

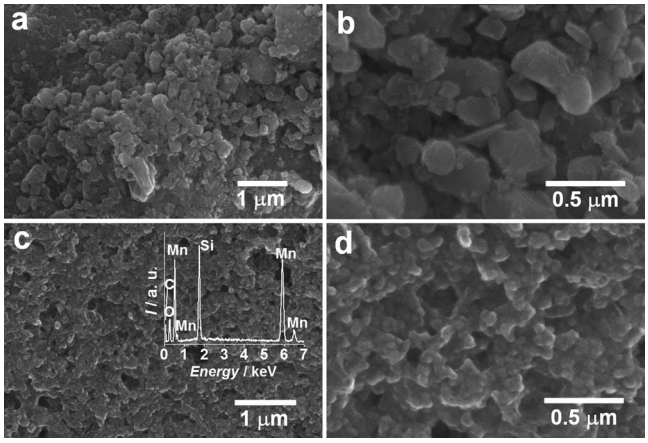

Figure 3. FE-SEM images of neat Li_2MnSiO_4 (a and b) and Li_2MnSiO_4/C composite (c and d). Inset of (c) shows an EDX plot of the Li_2MnSiO_4/C composite.

have shown that it crystalizes in different polymorphs with the following space groups: $Pmn2_1$, Pmnb, $P2_1/n$ and Pn.[21,22] The dominant, sharp, and intense diffraction peaks observed in the XRD patterns of both neat Li_2MnSiO_4 and the Li_2MnSiO_4/C (Fig. 2a) can be indexed to the orthorhombic crystal system with $Pmn2_1$ space group (ICSD-161305), indicating that the crystal structure of the neat silicate is preserved ongoing from the neat silicate to the composite with carbon. It can be seen from the XRD pattern that after the formation of the in-situ carbon coating on Li_2MnSiO_4, the diffraction peaks broadened significantly when compared to neat Li_2MnSiO_4. This indicates a decrease in particle size which implies a more open structure that can improve the kinetics of the Li-ion during charge/discharge and hence the capacity will also increase. The orthorhombic phase is a layered structure and is also iso-structural with β-Li_3PO_4 (tri-lithium phosphate) and therefore in Li_2MnSiO_4, Mn^{2+} ions occupy the tetrahedral sites within the $(SiO_4)^{4-}$ anionic silicate framework that replaces the $(PO_4)^{3-}$ anionic phosphate framework (the latter, as in β-Li_3PO_4). The lithium ions occupy the tetrahedral sites between the silicon and manganese tetrahedra. The lattice parameters of the Li_2MnSiO_4/C composite are: a = 6.407, b = 5.276 and c = 4.95 Å. A few weak intensity peaks arising from impurities such as Li_2SiO_3, MnO and Mn_2SiO_4 were also observed, and similar observations have been made in the past by other researchers for lithium orthosilicates.[10–18] From BET measurements, a surface area of 5 m^2 g^{-1} for the as-prepared neat Li_2MnSiO_4 was delineated whereas the Li_2MnSiO_4/C composite was characterized by a surface area of 60 m^2 g^{-1}. The twelve-fold enhancement in surface area ongoing from the neat Li_2MnSiO_4 to the Li_2MnSiO_4/C composite is a consequence of the carbon coating on Li_2MnSiO_4. Since the carbon coating on Li_2MnSiO_4 was generated in a single step, wherein starch transformed to carbon, whilst simultaneously the oxide crystallized, the carbon coats the Li_2MnSiO_4 crystallites and prevents the grain growth.

The Raman spectra of Li_2MnSiO_4/C composite and neat Li_2MnSiO_4 are shown in Fig. 2b. The Raman spectrum of neat Li_2MnSiO_4 shows only a single broad absorption at 609 cm^{-1} and this peak is seen at 650 cm^{-1} for the composite. This peak arises from the Si-O vibrational mode of the SiO_4 tetrahedra. The Raman spectrum of the composite also shows additional contributions from carbon coating in the 1200–1600 cm^{-1} wavenumber range. The deconvoluted Raman spectrum of the Li_2MnSiO_4/C composite in the 1000–1800 cm^{-1} wavenumber region is shown in the inset of Fig. 2b. This portion of the spectrum provides information about the nature of carbon coating in the composite. The fundamental D and G bands are centered at about 1332 and 1582 cm^{-1}, conforming to the sp^2 hybridized nature of the carbon bonding in the Li_2MnSiO_4/C composite.[17] The deconvoluted Gaussian components are observed at 1240, 1336, 1470 and 1587 cm^{-1}, and these are assigned as I, D, D" and G bands respectively, in concurrence with a previous report on a Li_2FeSiO_4/C composite, prepared from a microwave method using sucrose as the carbon source.[17] It has been observed in the past, that higher the peak intensity ratio of D and G bands (I_D/I_G), greater is the extent of ordering/crystallinity in the carbon coating.[17] Authors in this report[17] obtained a low value of ∼1.63 for the I_D/I_G ratio for a Li_2FeSiO_4/C composite and concluded that the carbon coating is amorphous. Similarly for the Li_2MnSiO_4/C composite here, we found I_D/I_G to be equal to 0.97, thus affirming that the carbon coating enwrapping the Li_2MnSiO_4 grains in the composite is also amorphous. The SEM images of neat Li_2MnSiO_4 (displayed in Figs. 3a and 3b), show the Li_2MnSiO_4 particles have irregular shapes and particle sizes are of the order of 0.1 to 0.5 μm. Low magnification SEM image of the Li_2MnSiO_4/C composite shown in Fig. 3c reveals a granular porous morphology. The corresponding high magnification image (Fig. 3d) shows the presence of interconnected aggregates separated by pores with dimensions varying from 10 to 80 nm. The uniformity of the texture indicates that the amorphous carbon is in all likelihood homogenously deposited over the Li_2MnSiO_4 grains. The Li_2MnSiO_4 particles (in the neat silicate, Fig. 3b), do not appear to be as well-connected as they are in the composite (Fig. 3d). The formation of Li_2MnSiO_4/C composite was also confirmed from energy dispersive X-ray analysis (EDX), as signals from the constituent elements: Li, Mn, Si, O and C were observed in the pattern, which is displayed in Fig. 3c.

The TEM image of the Li_2MnSiO_4/C composite shows dark grains of irregular shapes of Li_2MnSiO_4 surrounded by layers with a glazy contrast; the latter due to amorphous carbon (Fig. 4a). A HRTEM image of the composite (Fig. 4b) clearly reveals the lattice fringes arising from the orthorhombic crystal structure of Li_2MnSiO_4 and these fringes are flanked by amorphous carbon layers. An enlarged view of the lattice fringes is presented in Fig. 4c and the inter-planar spacing deduced from the image is ∼1.6 Å, which corresponds to the (400) plane of orthorhombic Li_2MnSiO_4.[18] Another lattice scale image of a Li_2MnSiO_4 grain oriented along the (011) plane is shown in Fig. 4d. The grain size of Li_2MnSiO_4 was estimated to be 18 nm

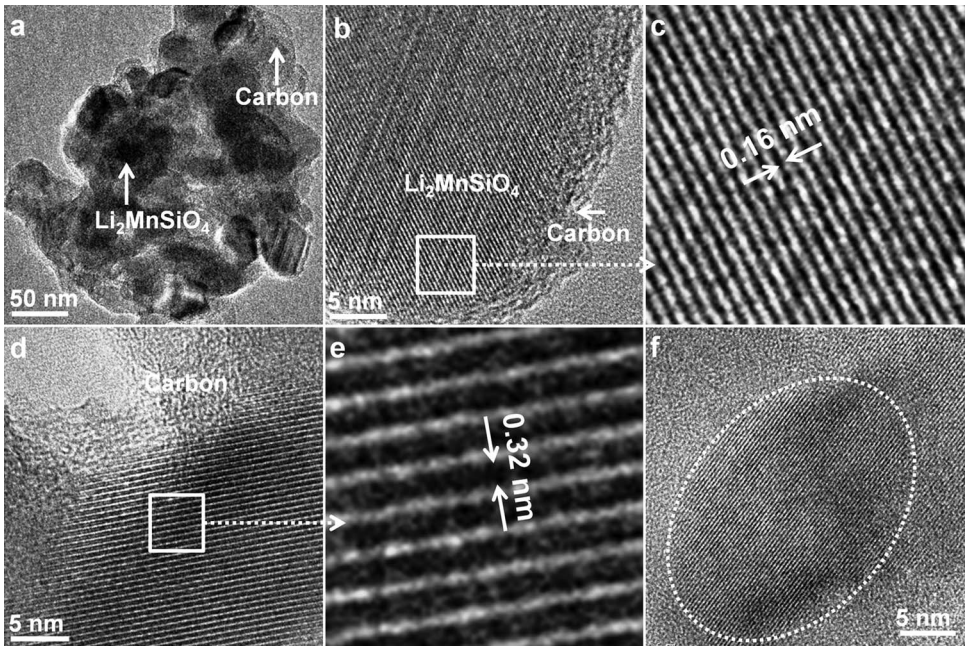

Figure 4. (a) A TEM image of a Li_2MnSiO_4/C composite, (b) a HRTEM image showing the amorphous carbon juxtaposed with crystalline Li_2MnSiO_4, (c) enlarged view of (b) showing the lattice fringes of Li_2MnSiO_4, (d,e) lattice scale images of a Li_2MnSiO_4 grain oriented along the (011) plane and (f) lattice scale image of Li_2MnSiO_4 used for grain size determination.

from Fig. 4f, wherein the dotted ellipse encapsulates a Li_2MnSiO_4 grain oriented along the (002) plane. The amorphous carbon layers are once again observed to form a sheath around the Li_2MnSiO_4 crystallite. Such a direct contact between the two entities is most beneficial, as the conductive carbon coating can allow rapid electron transport through the composite electrode, during electrochemical cycling.

C-AFM studies.— Fig. 5 shows the simultaneous topography and current images for a 1 μm × 1 μm region of an as-prepared electrode surface of the Li_2MnSiO_4/C composite. The topography of the composite shows a few large particulates and is almost featureless (Fig. 5a). The current image was generated by contacting a conductive tip with the electrode surface and a small bias voltage of 50 mV was applied between the tip and the substrate while the tip ran horizontally over the surface (Fig. 5b). In the current image, the bright regions arise from the high current domains and the dark regions represent low currents. A large number of bright spots are seen to be embedded in an insulating surface; the bright spots could be the carbon rich domains of the composite and the dark regions originate from the regions with relatively less carbon content. The maximum nanoscale current achieved in the composite is about 268 nA, indicating the good electronic current carrying ability of the composite. On the other hand, neat Li_2MnSiO_4 did not yield a current image, as the material was highly insulating. Such an increased ability to conduct electrons is achieved in the composite is due to a direct contact between the conducting carbon and insulating Li_2MnSiO_4 grains which in turn can facilitate Li^+ ion transfer and transport during electrochemical charge-discharge cycling. Point contact I-V curves were recorded at fifteen equidistant points on the current image, and the average I-V profile of the Li_2MnSiO_4/C composite is shown in Fig. 5c. A quasi-linear dependence of current on swept potential was confined to a voltage window of about −1.0 to + 1.0 V and thereafter, current tends to saturate.

Electrochemistry of Li-ion Cells.— The cyclic voltammograms (CV) of the Li_2MnSiO_4/C *versus* Li metal at a scan rate 0.05 mV s^{-1} are shown in Fig. 6a. During charging, the CV curve shows a small peak about +4.0 corresponds to the oxidation of Mn^{+2} to Mn^{+3} and a broad peak at 4.5 V which is attributed to Mn^{+3}/Mn^{+4}.[20–22] Another broad peak at ∼4.7 V in all likelihood is due to electrolyte decomposition, it may also be due to Mn^{+3}/Mn^{+4} but there is no report to date. In the discharging branch of the voltammogram, a broad peak is observed at +2.9 V, which corresponds to lithiation. Fig. 6b shows the galvanostatic charge-discharge curves of Li_2MnSiO_4/C and neat Li_2MnSiO_4 recorded at a C-rate of 0.05 (where 1C corresponds to complete charge or discharge for 1 h for one lithium; the carbon content was excluded for the calculation of C-rate) in the voltage range of 1.5–4.8 V. The composite exhibits an initial charge and discharge specific capacities of 328 mAh g^{-1} and 195 mAh g^{-1}, respectively; corresponding to almost 2 Li^+ extraction and ∼ 1.2 Li^+ insertion. In the first cycle the electrode material encountered an irreversible capacity loss of ∼ 40%. The poor irreversibility during the first cycle may be due to the formation of solid electrolyte interface (SEI) as some lithium ions are irreversibly consumed on charging.[18] Even after 30 cycles the Li_2MnSiO_4/C composite delivers a reversible capacity of 115 mAh g^{-1}, corresponds to an insertion of 0.73 Li^+ ions. Capacity fading with increase in the number of cycles can be due to any one or all of the following: (i) the gradual loss of the crystal structure, (ii) Jahn-Teller distortion induced in the intermediate containing the Mn^{3+} species and (iii) slow dissolution of manganese in the electrolyte.[23,24] Neat Li_2MnSiO_4 showed initial charge and discharge capacities, respectively, of 37 and 10.6 mAh g^{-1} (Fig. 6b). The effect of the in-situ carbon coating in (i) improving the Li^+ ion storage capacity and (ii) in endowing the orthosilicate with the ability to undergo repetitive charge-discharge cycles with lowered capacity loss is evident from the higher capacity and reduced capacity fading in composite relative to the neat orthosilicate. The composite also exhibits rate capabilities acceptable for battery applications (Fig. 6c) as at a 0.1 C-rate it gave a reversible specific capacity of 136.5 mAh g^{-1} corresponding to a ∼0.82 Li^+ reversible extraction/insertion for the first cycle. Further, at a 0.2 C-rate the Li_2MnSiO_4/C composite delivers a reversible specific capacity 119.6 mAh g^{-1} for the first cycle. In the case of neat Li_2MnSiO_4, the capacity is reduced to about 5 mAh g^{-1} after

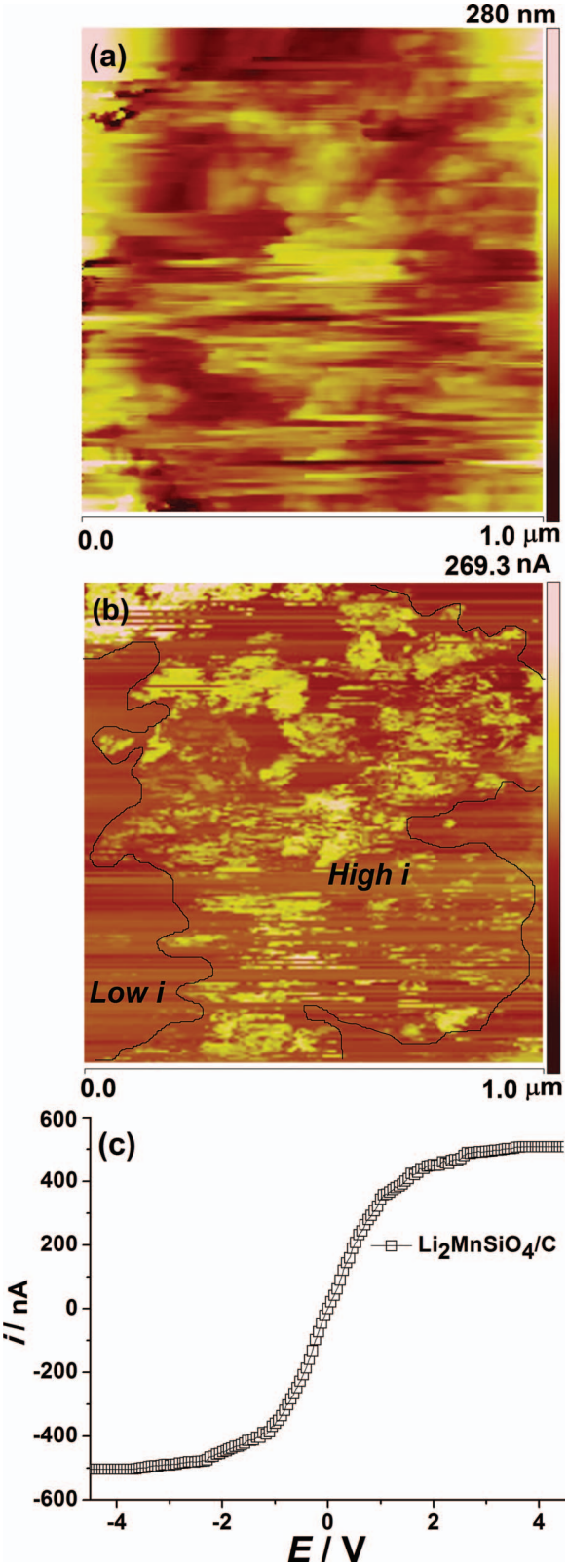

Figure 5. Simultaneous (a) topography and (b) current images of a Li_2MnSiO_4/C composite. (c) Averaged point contact I-V curve obtained after averaging I-V responses from 15 different spots on the current image shown in (b).

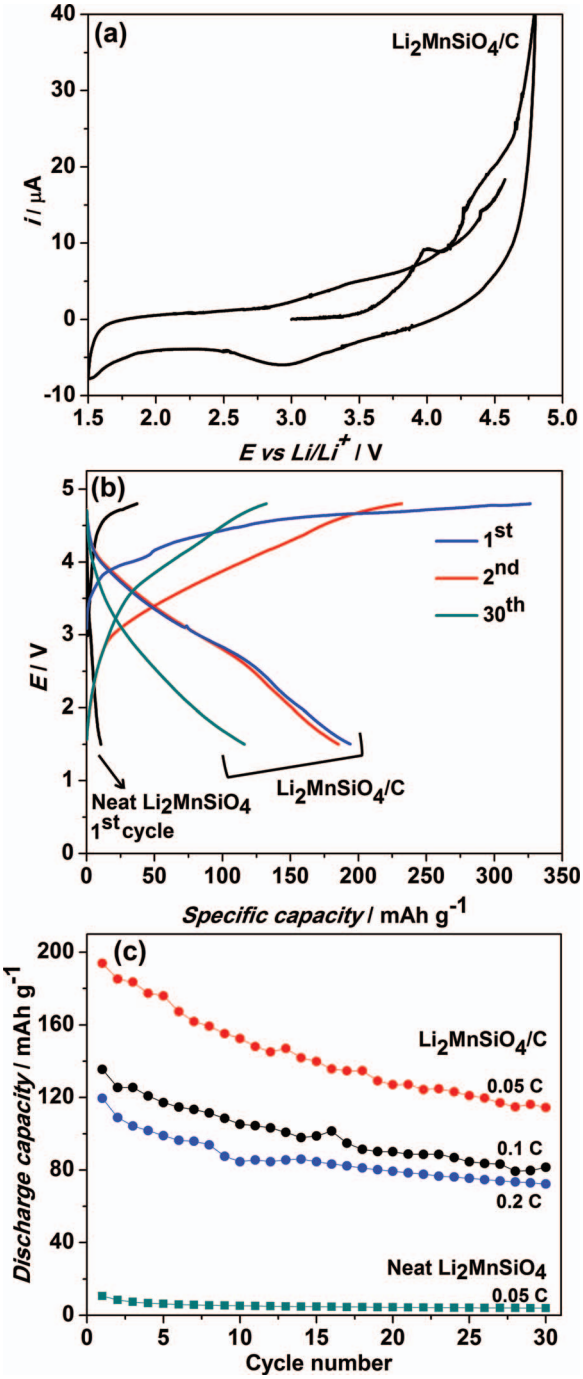

Figure 6. (a) Cyclic voltammogram of the Li_2MnSiO_4/C composite (b) galvanostatic charge-discharge curves of neat Li_2MnSiO_4 and Li_2MnSiO_4/C composite at a C-rate of 0.05 and (c) cyclability of neat Li_2MnSiO_4 and the Li_2MnSiO_4/C composite and rate capability of the composite.

30 cycles (Fig. 6c). Ex-situ XRD patterns of the cycled Li_2MnSiO_4/C composite (at different stages) are shown in Fig. 7. The ex-situ XRD pattern at 0.05 C-rate after the first cycle still shows traces of the main diffraction peaks of Li_2MnSiO_4 in contrast to some of the previous reports where the composite became completely amorphous.[12] After 30 cycles the ex-situ XRD pattern shows the composite to be completely amorphous.

Nyqvist plots of Li_2MnSiO_4/C composite and neat Li_2MnSiO_4 *versus* Li metal were shown in Fig. 8a. The measurements were performed over an applied frequency range of 100 kHz to 10 mHz, by using an ac amplitude of 10 mV. The Z" *versus* Z' curves for the

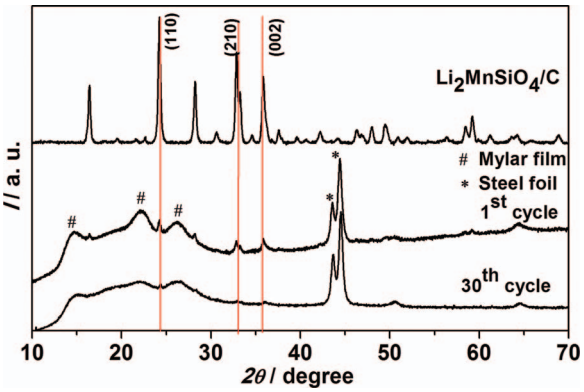

Figure 7. Ex-situ XRD patterns for the Li_2MnSiO_4/C composite after 1st and 30th cycles compared with the XRD pattern of as-prepared Li_2MnSiO_4/C composite.

Li_2MnSiO_4/C composite recorded at intermittent stages of charges are shown in Fig. 8b. All plots show one skewed semicircle followed by an inclined straight line; the latter is confined to the low frequency domain. The high frequency region where the curve touches the real axis corresponds to the electrolyte and electrodes resistance (R_e). The high to medium frequency range is ascribed to a parallel combination of charge transfer resistance (R_{CT}) and electrical double layer capacitance (C_{dl}), and the straight line originates from the diffusion of

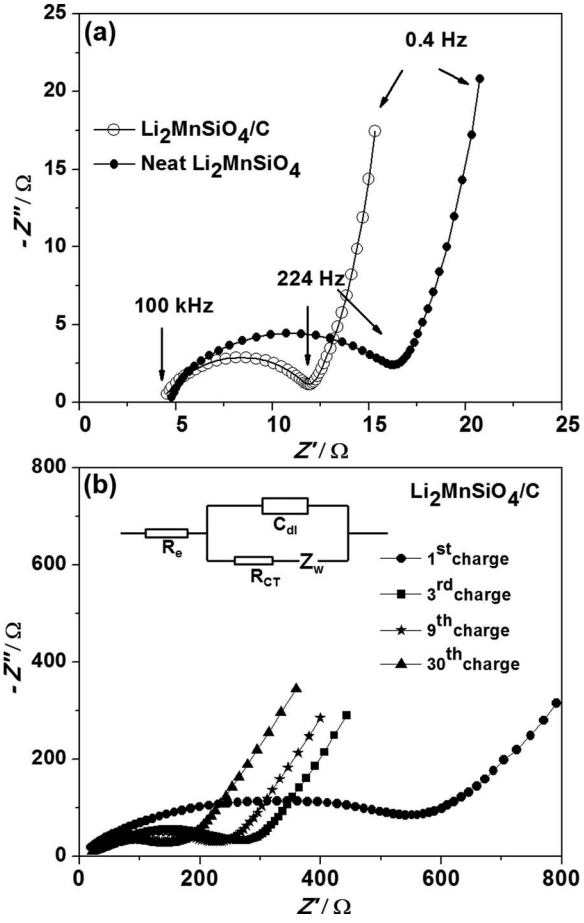

Figure 8. Nyqvist plots for the (a) Li_2MnSiO_4/C composite and neat Li_2MnSiO_4 at open-circuit potential and (b) at the intermittent fully charged states of the Li_2MnSiO_4/C composite and; inset of (b) shows the equivalent circuit used for fitting the data.

Table I. Equivalent circuit parameters for the Z" versus Z' plots displayed in Fig. 8.

Sample	R_e (Ω)	R_{CT} (Ω)	C_{dl} (μF)	σ (of Zw, $m\Omega^{-1}$)
Neat Li_2MnSiO_4	4.6	16.5	4.2	7.5
Li_2MnSiO_4/C	4.3	12	4.8	9.7
Li_2MnSiO_4/C				
After 1st charge	19.8	541.2	4.15	2.05
After 3rd charge	26	268.2	1.53	2.6
After 9th charge	29.5	226.4	1.76	3.4
After 30th charge	21.6	143	2.6	2.9

charged species through the bulk of the electrode material. Fig. 8a shows that the as fabricated cell of Li_2MnSiO_4/C composite exhibits a lower charge-transfer resistance (12 Ω) as compared to neat Li_2MnSiO_4 (16.5 Ω), indicating that the carbon coating facilitates charge transfer at the interface which can lead to higher capacity as observed herein. The low frequency response, which arises from Warburg impedance (Z_w) shows a slant poised at almost 90° with respect to the real component of impedance (Z'). Such a response, is characteristic of a dominant capacitive contribution to impedance, and since the slope does not change significantly ongoing from the neat silicate to the composite, it is apparent that it is the active material which controls the nature of the response, especially in the low frequency region. The equivalent circuit shown in the inset of Fig. 8b, was used for fitting the experimental data. The values for the circuit components are summarized in Table I. Most interestingly, the conductance component of Z_w has a value of 9.7 $m\Omega^{-1}$, for the composite and it is 7.5 $m\Omega^{-1}$ for the neat silicate (Fig. 8a), indicating that even in the low frequency region, the composite offers less impeded pathways for ion movement, as compared to the neat silicate. Fig. 8b shows the Nyqvist plots of Li_2MnSiO_4/C in the fully charged state (at 0.05 C-rate) of the first, ninth and thirtieth cycles. After the 1st charge, the cell shows a huge increase in R_{CT} (541 Ω) this could be due to the formation of sold electrolyte interface whereby some lithium ions are consumed irreversibly.[25] However, as the cycle number was raised successively from 3 to 9 to 30, the charge transfer resistance decreased to 133 Ω. The radius of the semicircle was observed to shrink as a function of cycle number. Moreover, the difference in radius between the first cycle and the second circle is larger than that between the second cycle and the tenth cycle, revealing that the passivating film which is formed during the first charge/discharge process is stable during the subsequent charge/discharge cycles and offers less resistance to ion transfer and transport. The slope of the straight-line curve corresponding to Warburg impedance changes from 1.08 to 1.03 ongoing from first to the thirtieth charge, indicating a changeover from capacitive to a resistive behavior in the low frequency regime. Simultaneously, with cycling, the magnitude of Z_w also increased from 2.05 to 2.9 $m\Omega^{-1}$, reaffirming the ability of the composite to be more amenable for transport of Li-ions in the low frequency domain.

Conclusions

An in-situ carbon coated Li_2MnSiO_4/C composite was prepared by a facile nanocomposite gel precursor route, wherein starch served as the carbon source, and was introduced along with the active battery material precursors to yield a homogeneous product upon elevated temperature annealing. EDX, Raman, HRTEM and XRD studies confirmed the formation of Li_2MnSiO_4/C composite. HRTEM studies revealed that Li_2MnSiO_4 grains with an orthorhombic crystal structure are surrounded by conductive carbon layers. C-AFM showed the presence of interlinked high current regions in the composite. An initial specific charge capacity of 330 mAh g^{-1} at a 0.05 C-rate was achieved in the Li_2MnSiO_4/C composite, which is relatively higher than some of the values reported for Li_2MnSiO_4. Although capacity fading was registered in the composite, but it retained a reversible capacity of 115 mAh g^{-1} (at 0.05 C-rate) even after 30 cycles. Electrochemical

impedance spectral analysis also revealed that charge transfer resistance does not increase significantly upon cycling for the composite and R_{CT} was also found to be lower than that of neat Li_2MnSiO_4; the latter indicating a direct contact between Li_2MnSiO_4 grains and carbon which leads to facile charge conduction. The scalability of the synthetic route for preparing electrodes, the retention of a reasonably high charge-discharge capacity with cycling, the moderate rate capability of the composite and most importantly, the ecologically non-toxic nature of Li_2MnSiO_4 indicate the promise of the Li_2MnSiO_4/C composite prepared herein as cathodes for practical Li-ion batteries.

Acknowledgments

We thank International Advanced Research Center for Powder Metallurgy and New Materials (ARCI) and Indo-French Center for the Promotion of Advanced Research (CEFIPRA) for financial support.

References

1. S. Venkatraman and A. Manthiram, *Chem. Mater.*, **15**, 5003 (2003).
2. S. Choi and A. Manthiram, *J. Solid State Chem.*, **164**, 332 (2002).
3. Y. Wang, P. He, and H. Zhou, *Energy Environ. Sci.*, **4**, 805 (2011).
4. C. Lyness, B. Delobel, A. R. Armstrong, and P. G. Bruce, *Chem. Commun.*, 4890 (2007).
5. Z. L. Gong, Y. X. Li, and Y. Yang, *J. Power Sources*, **174**, 524 (2007).
6. A. Nyten, A. Abouimrane, M. Armand, T. Gustafsson, and J. O. Thomas, *Electrochem. Commun.*, **7**, 156 (2005).
7. C. Sirisopanaporn, C. Masquelier, P. G. Bruce, A. R. Armstron, and R. Dominko, *J. Am. Chem. Soc.*, **133**, 1263 (2011).
8. X. Huang, X. Li, H. Wang, Z. Pan, M. Qu, and Z. Yu, *Electrochim. Acta*, **55**, 7362 (2010).
9. M. Saiful Islam, R. Dominko, C. Masquelier, C. Sirisopanaporn, A. R. Armstrongd, and P. G. Bruce, *J. Mater. Chem.*, **21**, 9811 (2011).
10. R. Dominko, M. Bele, M. Gaberscek, A. Meden, M. Remskar, and J. Jamnik, *Electrochem. Commun.*, **8**, 217 (2006).
11. M. E. Arroyo-de Dompablo, M. Armand, J. M. Tarascon, and U. Amador, *Electrochem. Commun.*, **8**, 1292 (2006).
12. Y. X. Li, Z. L. Gong, and Y. Yang, *J. Power Sources*, **174**, 528 (2007).
13. R. Dominko, M. Bele, A. Kokalj, M. Gaberscek, and J. Jamnik, *J. Power Sources*, **174**, 457 (2007).
14. I. Belharouak, A. Abouimrane, and K. Amine, *J. Phys. Chem. C*, **113**, 20733 (2009).
15. N. Kuganathan and M. S. Islam, *Chem. Mater.*, **21**, 5196 (2009).
16. V. Aravindan, K. Karthikeyan, J. W. Lee, S. Madhavi, and Y. S. Lee, *J. Phys. D: Appl. Phys.*, **44**, 152001 (2011).
17. T. Muraliganth, K. R. Stroukoff, and A. Manthiram, *Chem. Mater.*, **22**, 5754 (2010).
18. V. Aravindan, K. Karthikeyan, K. S. Kang, W. S. Yoon, W. S. Kim, and Y. S. Lee, *J. Mater. Chem.*, **21**, 2470 (2011).
19. D. Rangappa, K. D. Murukanahally, T. Tomai, A. Unemoto, and I. Honma, *Nano Lett.*, **12**, 1146 (2012).
20. P. Ghosh, S. Mahanty, and R. N. Basu, *J. Electrochem. Soc.*, **156**, A677 (2009).
21. M. E. Arroyo-de Dompablo, R. Dominko, J. M. Gallardo-Amores, L. Dupont, G. Mali, H. Ehrenberg, J. Jamnik, and E. Moran, *Chem. Mater.*, **20**, 5574 (2008).
22. H. Duncan, A. Kondamreddy, P. H. J. Mercier, Y. Le Page, Y. Abu-Lebdeh, M. Couillard, P. S. Whitfield, and I. J. Davidson, *Chem. Mater.*, **23**, 5446 (2011).
23. K. A. Walz, C. S. Johnson, J. Genthea, L. C. Stoiber, W. A. Zeltnera, M. A. Anderson, and M. M. Thackeray, *J. Power Sources*, **195**, 4943 (2010).
24. R. Vidu and P. Stroeve, *Ind. Eng. Chem. Res.*, **43**, 3314 (2004).
25. S. S. Zhang, K. Xu, and T. R. Jow, *J. Electrochem. Soc.*, **149**, A1521 (2002).